



## RESEARCH LETTER

10.1002/2016GL071767

## Key Points:

- Analyses of Argo float temperature and satellite energy flux data illustrate redistribution and variations of heat storage with ENSO
- Monthly ocean analyses reveal large-scale ocean heat content variations, while yearly analyses reveal variations in Earth's energy storage
- A 1°C increase of the Niño3.4 index corresponds to an increase of ~3.4 ZJ in Earth's energy storage, modulating the ~114 ZJ/decade trend

## Correspondence to:

G. C. Johnson,  
gregory.c.johnson@noaa.gov

## Citation:

Johnson, G. C., and A. N. Birnbaum (2017), As El Niño builds, Pacific Warm Pool expands, ocean gains more heat, *Geophys. Res. Lett.*, *44*, 438–445, doi:10.1002/2016GL071767.

Received 28 OCT 2016

Accepted 25 DEC 2016

Accepted article online 28 DEC 2016

Published online 13 JAN 2017

Published 2016. This article is a US Government work and is in the public domain in the United States of America.

## As El Niño builds, Pacific Warm Pool expands, ocean gains more heat

Gregory C. Johnson<sup>1</sup>  and Abigail N. Birnbaum<sup>1,2</sup> 

<sup>1</sup>Pacific Marine Environmental Laboratory, NOAA, Seattle, Washington, USA, <sup>2</sup>College of Engineering, Cornell University, Ithaca, New York, USA

**Abstract** El Niño–Southern Oscillation (ENSO) effects substantial redistributions of ocean temperature, both horizontal and vertical, on interannual time scales, especially in the Pacific Ocean. Analyses of monthly Argo-based ocean temperature maps illustrate large-scale ocean heat content redistributions with ENSO. They quantify a globally averaged sea surface temperature warming of ~0.1°C with a 1°C increase of the Niño3.4 index (a moderate El Niño), a substantial perturbation to the 0.13°C decade<sup>-1</sup> trend in sea surface temperature. Monthly satellite-based estimates of Earth's energy imbalance suggest that a 1°C increase of the Niño3.4 index corresponds to an increase of ~3.4 ZJ in Earth's energy storage, more gently modulating the longer-term ~114 ZJ decade<sup>-1</sup> trend. Yearly global ocean heat content estimates based on ocean temperature data, with their reduced uncertainties compared to monthly maps, reveal interannual variations in Earth's energy storage that correspond well with satellite-based estimates.

### 1. Introduction

El Niño–Southern Oscillation (ENSO) events involve the redistribution and modulation of ocean temperature worldwide [Roemmich and Gilson, 2011], especially in the upper few hundred meters of the tropical Pacific Ocean [Meinen and McPhaden, 2000]. When Pacific westerly trade winds relax during El Niño, the western tropical Pacific warm pool spreads eastward near the surface and shoals in the west, and eastern equatorial Pacific upwelling is reduced [McPhaden et al., 2006]. Globally averaged surface temperatures are affected by ENSO, becoming relatively warmer during El Niño and cooler during La Niña events, which modulates the long-term warming on interannual time scales [Foster and Rahmstorf, 2011]. Global integrals of top of the atmosphere (TOA) net energy fluxes from satellite data have also suggested a link between variations in Earth's energy imbalance and ENSO, with TOA net fluxes relatively high for several months prior to and low for several months after the 1997–1998 El Niño [Wong et al., 2006] and a similar pattern apparent for the 2009–2010 El Niño [Loeb et al., 2012]. In contrast, analysis of net fluxes estimated from the time derivative of in situ estimates of 0–500 m global ocean heat content from 2004 to 2011 suggested that ocean heat gain may be relatively low during El Niño events and high during La Niña events [Roemmich and Gilson, 2011].

For direct comparison of ocean and satellite data, rather than taking time derivatives of the ocean heat storage anomalies as is done in the studies above, we choose to time-integrate the TOA net flux anomalies, yielding TOA net energy storage anomalies. We find that for both satellite and ocean-based estimates, variations in Earth's energy storage peak in phase with El Niño, and trough with La Niña, resulting in a striking correlation between TOA net energy storage anomalies and the Niño3.4 index. We estimate a global energy perturbation of 3.4 ZJ (1 ZJ = 10<sup>21</sup> J) for a 1°C Niño3.4 anomaly. We further quantify patterns of ocean warming and cooling with ENSO through analysis of 150 months of global ocean temperature data, illustrating where the ocean stores additional heat during El Niño.

### 2. Data

We analyze a monthly gridded ocean temperature and salinity data set [Roemmich and Gilson, 2009], with a major update through 2014, and monthly updates from January 2015 through June 2016. For this product Argo temperature and salinity data only are mapped on a 1° latitude by 1° longitude grid, centered on half-degrees from 64.5°S to 64.5°N. Marginal seas are excluded from the mapping. The vertical coordinate is pressure, with 58 levels from the surface to 2000 dbar, and vertical resolution coarsening with increasing pressure. The data set was downloaded in July 2016 from [http://sio-argo.ucsd.edu/RG\\_Climatology.html](http://sio-argo.ucsd.edu/RG_Climatology.html).

We also use an updated [Blunden and Arndt, 2016] global mean annual ocean heat content anomaly (OHCA) time series [Lyman and Johnson, 2014] for 0–1800 m over 1993.5–2015.5.

We further employ the Energy Balanced and Filled (EBAF2.8) satellite-observed monthly global estimates of TOA net energy fluxes from CERES (Clouds and the Earth's Radiant Energy System). These data were downloaded in July 2016 from <http://ceres.larc.nasa.gov/products.php?product=EBAF-TOA>.

As a gauge of the amplitude and phase of ENSO we use the monthly Niño3.4 index, which is the temperature anomaly relative to 30 year monthly mean values recalculated at 5 year intervals in the Niño 3.4 area (a rectangle bounded by 5°S and 5°N in latitude and 170°W and 120°W in longitude). The Niño3.4 index was also downloaded in July 2016 from [http://www.cpc.ncep.noaa.gov/products/analysis\\_monitoring/ensostuff/detrend.nino34.ascii.txt](http://www.cpc.ncep.noaa.gov/products/analysis_monitoring/ensostuff/detrend.nino34.ascii.txt).

### 3. Analysis

For our analysis of the Argo gridded data set, we first use the location, temperature, practical salinity, and pressure ( $p$ ) values to compute, using TEOS-10 (<http://www.teos-10.org/index.htm>) [Intergovernmental Oceanographic Commission et al., 2010], absolute salinity ( $S_A$ ), and conservative temperature ( $\Theta$ ) at every grid point and time. At each grid point we fit, to the 150 month time series of  $S_A$  and  $\Theta$ , by least squares regression to the following equation:

$$a_m + a_t \cdot (t - \langle t \rangle) + a_{s1} \cdot \sin(2 \cdot \pi \cdot t) + a_{c1} \cdot \cos(2 \cdot \pi \cdot t) + a_{s2} \cdot \sin(4 \cdot \pi \cdot t) + a_{c2} \cdot \cos(4 \cdot \pi \cdot t) + a_n \cdot \text{Niño3.4}$$

where  $t$  is the time in years,  $\langle \rangle$  indicates a time average, and Niño3.4 is the time-varying Niño3.4 index. The regression coefficients give  $a_m$  the mean value,  $a_t$  the linear temporal trend relative to the central date of the time series,  $a_{s1}$  and  $a_{c1}$  the annual harmonics,  $a_{s2}$  and  $a_{c2}$  the semiannual harmonics, and  $a_n$  the linear response to the Niño3.4 index. We interpret the mean values from this fit as representative of the time-mean state, and the mean values plus the Niño3.4 response coefficients as representative of moderate (with a Niño3.4 index of 1°C) El Niño conditions. We study changes of  $\Theta$  and ocean heat content ( $Q$ ) anomalies on pressure surfaces and within pressure layers, respectively. Here  $Q = \int 1/g \cdot c_p \cdot \Theta dp$ , where  $c_p = 3991.8680 \text{ J kg}^{-1} \text{ K}^{-1}$  is the specific heat of seawater for use with  $\Theta$ ,  $\int dp$  indicates an integral over the layer versus pressure, and  $g$  is the acceleration due to gravity. We also globally volume-integrate monthly values of OHCA, and fit a linear temporal trend relative to the central date of the resulting time series along with annual and semiannual harmonics. We do not regress these global volume-integrated OHCA values against the Niño3.4 index to allow for a comparison against that index.

We similarly analyze the monthly TOA net energy flux data, fitting a mean value along with annual and semiannual harmonics to those values from July 2002 through February 2016. We choose that starting date because it is the first month when both CERES Terra and Aqua satellites were online. Prior to July 2002, when CERES Aqua was not yet operational, TOA net energy storage anomalies and the Niño3.4 index are not as well correlated (Figure 1a). We fit only the mean to the TOA net energy fluxes compared to a mean and a trend to the OHCA values because the former are the time derivatives of the latter (neglecting variations in energy storage by the land, deeper ocean, atmosphere, and ice and snow). Furthermore, we omit the Niño3.4 index in the regression to the monthly TOA net energy flux data. That omission allows for further exploration of interannual variability, particularly the connection between Earth's energy storage anomalies and ENSO. We then remove the resulting fit from the TOA net energy flux data and time-integrate the residuals to obtain a time series of monthly TOA net energy storage anomalies that can be compared directly with the OHCA values.

### 4. Results

TOA net energy storage anomalies from the time integrals of CERES TOA net energy flux data after removal of a mean and seasonal cycle from July 2002 to February 2016 are correlated at 0.72 with the Niño3.4 index over that same time period (Figure 1a). Correlation is maximum at zero time-lag, with a 1°C Niño3.4 index value equivalent to a 3.4 ZJ ocean heat gain. Positive net TOA energy flux is the signature of a warming climate, vital to understanding changes in the climate system including its response to radiative forcing and sea level rise [Rhein et al., 2013]. Variations in the rate of warming are also of high interest.

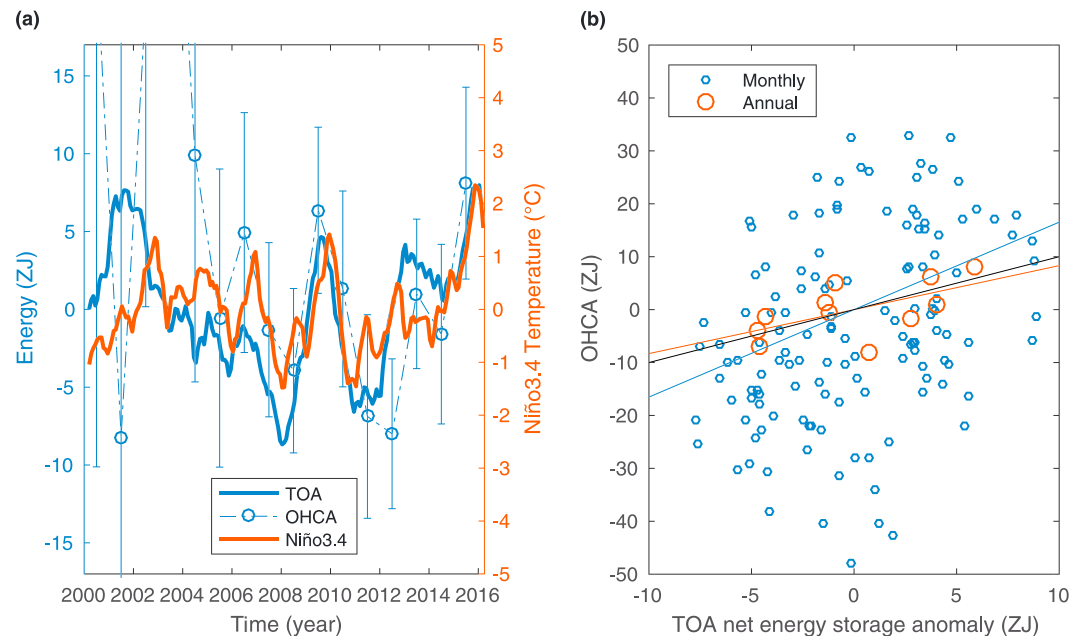


**Figure 1.** Relations among global volume-integrated ocean heat content anomalies (OHCA), globally averaged top of atmosphere (TOA) net energy storage anomalies in ZJ ( $1 \text{ ZJ} = 10^{21} \text{ J}$ ), and the Niño3.4 index (in  $^{\circ}\text{C}$ ) on monthly and annual time scales. (a) Time series of the Niño3.4 index (thick orange line, right axis) with TOA net energy storage anomalies from time-integrated CERES net TOA energy flux anomalies (thick blue line, left axis) and yearly OHCA (blue o's, thin dash-dotted line, with standard error of the mean range bars, left axis). (b) Scatterplot of monthly 0–1975 dbar (small blue circles) and yearly 0–1800 dbar (large orange circles) OHCA compared with TOA net energy storage anomalies averaged over the appropriate months or years, respectively. Slopes of the fits of these data using TOA net energy storage anomalies as the independent variable (colored lines) and a slope of unity (black line) are displayed. Seasonal cycles have been removed from all variables.

To put these results into context, a recently estimated [Johnson *et al.*, 2016] 2005–2015 time-averaged TOA net energy flux of  $0.71 (\pm 0.10) \text{ W m}^{-2}$  applied over the surface area of Earth based on in situ observations (mostly Argo data) is equivalent to an energy gain of about  $114 \text{ ZJ decade}^{-1}$ , and the standard deviation of Niño3.4 is  $0.79^{\circ}\text{C}$  over January 1950 to June 2015. Hence, even when Niño3.4 values are twice their standard deviation, the perturbation in net energy storage would be about  $5.4 \text{ ZJ}$ , or 5% of the decadal increase. ENSO thus modulates the mean long-term average energy storage rate over shorter time scales, but not does overwhelm it. Since sea levels rise as the oceans warm, ENSO events also temporarily modulate globally averaged sea level rise rates, with contributions of similar magnitude from land water storage related to these events [Piecuch and Quinn, 2016]. However, sea level variations during some ENSO events appear to be more influenced by land water storage, for example, the 2010–2011 La Niña [Fasullo *et al.*, 2013]. Some studies have even suggested that ENSO-related sea level variations are dominated by land water storage effects [Cazenave *et al.*, 2012]. In contrast, the rise in global surface temperatures is much more strongly modulated by ENSO [Foster and Rahmstorf, 2011].

Analyzing monthly variations of global volume-integrated OHCA using in situ data from the Argo array alone is more tenuous [Trenberth *et al.*, 2016]. The correlation of monthly Argo estimates of volume-integrated OHCA from January 2005 through February 2016 (with seasonal cycle and trend removed) with TOA net energy storage anomalies is only 0.36 (Figure 1b), and the slope of a regression using the TOA values as the independent variable is 1.65. This exceedance of unity is to be expected when regressing the relatively noisy in situ monthly global OHCA estimates against the more precise CERES TOA net energy storage anomalies. Over seasonal time scales oceanic heat storage is the primary buffer for variations in Earth's energy imbalance, although atmospheric heat storage does play a secondary role [Trenberth *et al.*, 2001]. Inclusion of monthly changes in atmospheric heat storage might increase the correlation slightly but could not possibly account for even a small fraction of the large monthly changes in ocean heat content.

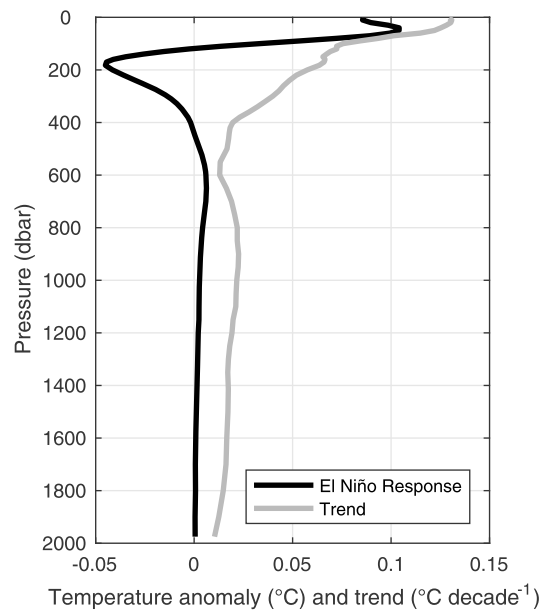


**Figure 2.** Global area-averaged ocean temperature response to El Niño and decadal trend versus pressure. The response (black line) is for moderate El Niño (Niño3.4 = 1°C) minus neutral (Niño3.4 = 0°C) conditions (black line). The decadal trend (grey line) has the seasonal cycle and Niño3.4 regression removed.

*et al.*, 2015]. By fitting a seasonal cycle, a trend, and a linear response to the Niño3.4 index [Trenberth and Stepaniak, 2001] to a monthly ocean temperature climatology [Roemmich and Gilson, 2009], we quantify that global area-averaged ocean temperature anomalies associated with ENSO reach about 0.1°C in the upper 60 dbar (Figure 2) for Niño3.4 = 1°C relative to ENSO neutral conditions. Hence, when Niño3.4 values are twice their standard deviation, the perturbation in sea surface temperature would be about 0.16°C, roughly 133% of the decadal increase of 0.12°C decade<sup>-1</sup>. Hence, ENSO has over an order of magnitude smaller effect on variations in the global energy storage relative to its long-term rate of increase than on globally averaged surface temperature variations relative to their long-term warming rate [Foster and Rahmstorf, 2011].

The surface warm anomalies during El Niño decrease rapidly with increasing depth (Figure 2) until reaching zero by about 120 dbar (1 dbar ~ 1 m). The anomalies are negative from 120 to 440 dbar, with a peak anomaly reaching almost -0.05°C at 180 dbar. Deeper than 440 dbar, the ocean warms in the global average during El Niño, with peak amplitude of about 0.007°C near 600 dbar. This phenomenon is documented in a previous analysis of a shorter time series [Roemmich and Gilson, 2011], but 150 months of data including a recent strong El Niño [Blunden and Arndt, 2016] motivate an analysis of spatial patterns of the linear response of OHCA to the Niño3.4 index in three pressure layers: the near-surface from 0 to 120 dbar, the subsurface from 120 to 440 dbar, and intermediate depths from 440 to 1975 dbar.

The OHCA response to El Niño in the tropical Pacific near-surface 0–120 dbar layer (Figure 3a) is as expected, with warm waters shifting from west to east, and from north to south, in zonally elongated patterns [Meinen and McPhaden, 2000]. The dominant feature is a warming in the eastern tropical Pacific, just south of the equator, with a maximum of about 0.9 GJ m<sup>-2</sup> (1 GJ = 10<sup>9</sup> J) located around 3°S, 125°W. There is also a secondary near-equatorial zonally elongated warming in the northeastern tropical Pacific with a maximum of about 0.7 GJ m<sup>-2</sup> at around 10°N, 120°W. The western tropical Pacific cooling patch north of the equator is smaller in area, with a minimum of about -0.8 GJ m<sup>-2</sup> just east of the Philippines. In the subsurface 120 to 440 dbar layer (Figure 3b) the response is qualitatively similar to that above, except that cooling dominates, as in the global average (Figure 2). Western tropical Pacific cooling is the strongest signal, with minima < -1 GJ m<sup>-2</sup> both east of the Philippines and the Solomon Islands. Eastern tropical Pacific warming in this layer has a maximum value of >0.4 GJ m<sup>-2</sup> in the Southern Hemisphere, smaller than that in the

In contrast, the better constrained global annual volume-integrated 0–1800 m OHCA values [Johnson *et al.*, 2016] and yearly means of TOA net energy storage anomalies for 2005–2015 are correlated at 0.60 (Figure 1b), with a regression slope of 0.83 (again using the TOA values as the independent variable). This relation is much closer to unity, consistent with the tighter correlation and the dominant role of the upper ocean in energy storage in the climate system [Johnson *et al.*, 2016]. Annual volume-integrated OHCA uncertainties decrease with time as the Argo array fills in, demonstrating the value of a global Argo array in climate studies (Figure 1a). Pre-2005 volume-integrated annual 0–1800 m OHCA values, estimated during a period when Argo was not yet even sparsely global, have large uncertainties, are noisy, and deviate from both TOA net energy storage anomalies and the Niño3.4 index.

While noisy for global integrals (Figure 1b) [Trenberth *et al.*, 2016], the monthly Argo maps are quite well suited to looking at spatial patterns of variability associated with ENSO [Roemmich and Gilson, 2011] and decadal trends [Roemmich

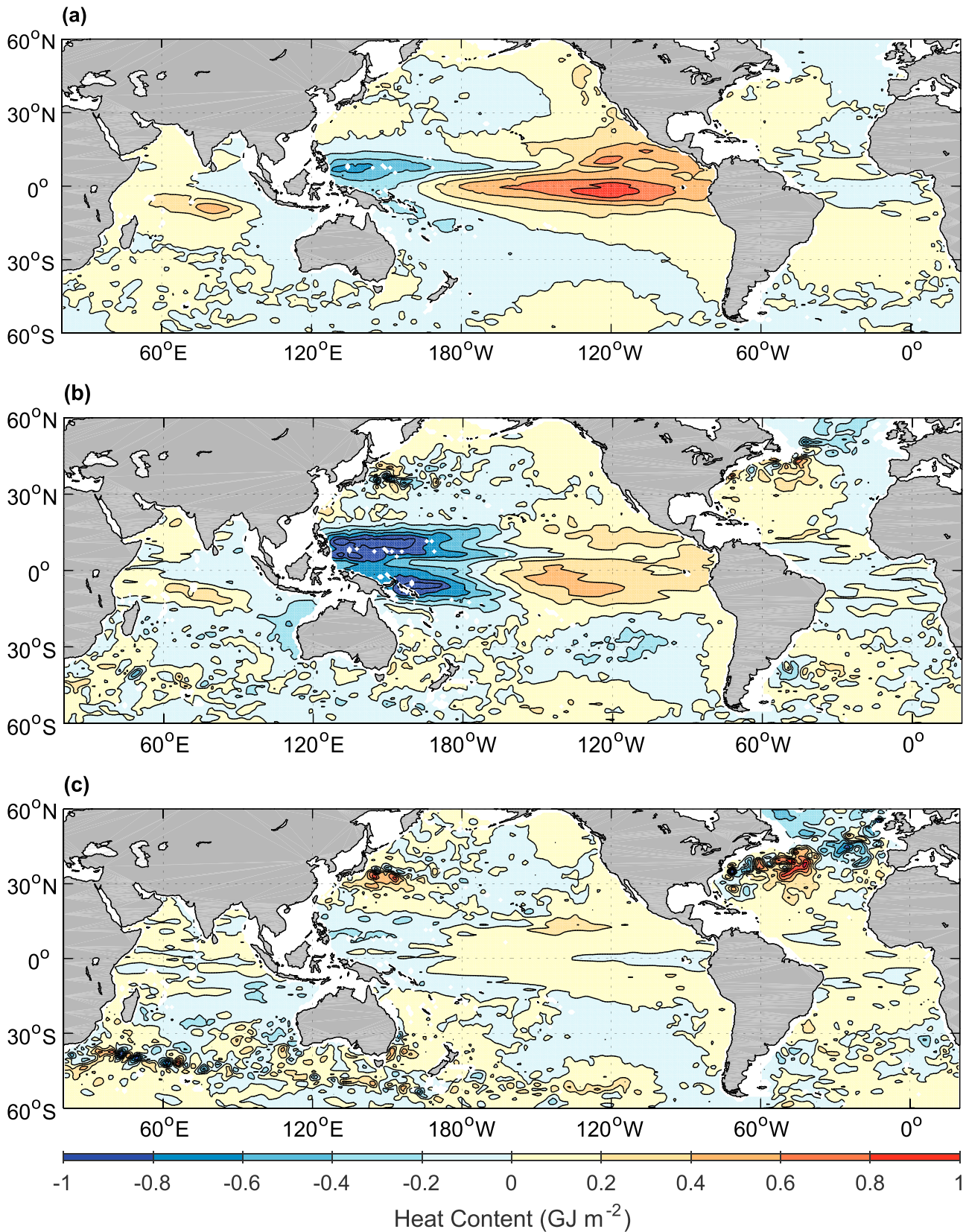


**Figure 3.** Maps of ocean heat content anomalies (OHCA) in  $\text{GJ m}^{-2}$  ( $1 \text{ GJ} = 10^9 \text{ J}$ ) for El Niño (Niño3.4 =  $1^\circ\text{C}$ ) minus neutral conditions integrated over three pressure layers: (a) near-surface, 0–120 dbar; (b) subsurface, 120–440 dbar; and (c) intermediate, 440–1975 dbar.

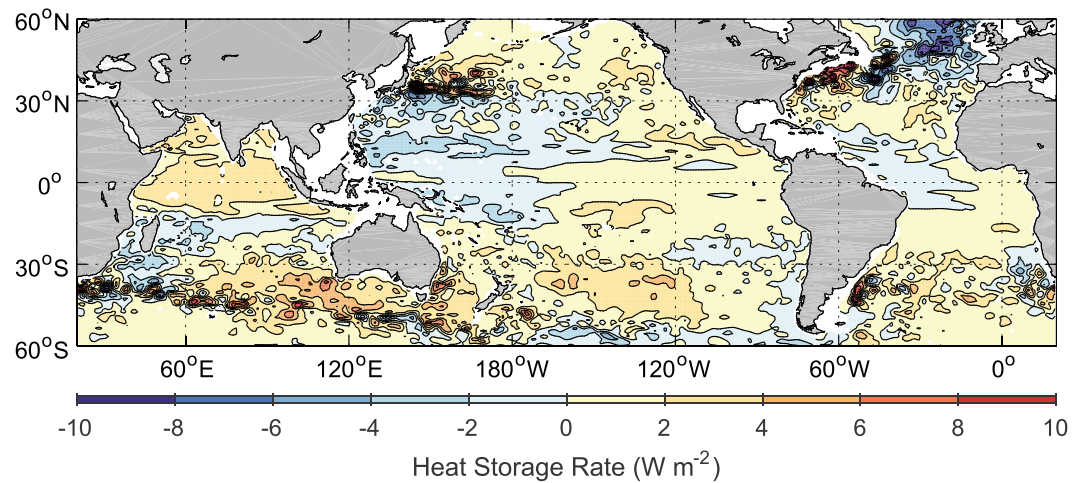


**Figure 4.** Map of ocean heat content anomaly (OHCA) trends ( $\text{W m}^{-2}$ ) integrated from 0 to 1975 dbar. The seasonal cycle and a Niño3.4 linear regression have been removed.

near-surface layer above. In the intermediate 440 to 1975 dbar layer (Figure 3c), the response is again similar to the layers above, although attenuated and with warming once again dominant in the global average (Figure 2).

Cooling in the eastern Indian Ocean with El Niño in all layers (Figure 3) is consistent with shrinking of the Indo-Pacific warm pool during El Niño [Wang and Mehta, 2008]. The western Indian Ocean warms slightly in all layers. The zonally elongated warming at around  $8^{\circ}\text{S}$  across much of the basin indicates a northward shift of the thermocline ridge that forms the northern edge of the westward flowing South Equatorial Current during El Niño [Lumpkin and Johnson, 2013], likely related to variations in the Indonesian Throughflow [Sprintall et al., 2014].

The Pacific warms off the west coasts of the Americas and cools slightly in the center of the subtropics in all layers (Figure 3), similar to the sea surface temperature signature of the warm phase of the Pacific Decadal Oscillation (PDO) [Newman et al., 2016]. The large area of slight warming in the subpolar South Pacific, centered at about  $45^{\circ}\text{S}$ ,  $130^{\circ}\text{W}$ , is likely owing to an atmospheric Rossby wave train associated with eastern tropical Pacific warming during El Niño [Ciasto et al., 2015]. The meridional dipole off Japan, with warming to the north and cooling to the south in the subsurface and intermediate layers, suggests a weakening of the Kuroshio extension. However, this change may be more related to the PDO, which is sometimes referred to as decadal ENSO, although the interaction is more complex [Newman et al., 2016].

Subtropical waters of the South Atlantic and western North Atlantic warm in the near-surface layer with El Niño, while the tropics cool (Figure 3). In the subsurface layer the cooling extends to the eastern tropics and subtropics, whereas in the intermediate layer, the whole area mostly warms. In these two deeper layers, the North Atlantic Current warms strongly (along with most of the western boundary current extensions), whereas the subpolar North Atlantic cools in all layers. The subpolar cooling is owing to cold conditions during 2015, coincident with the strong El Niño, but likely caused by other factors [Duchez et al., 2016]. Finally, in the intermediate layer, much of the Southern Ocean south of the Antarctic Circumpolar Current appears to warm with El Niño.

The global area-averaged decadal (January 2005 to June 2016) ocean temperature trend with the seasonal cycle and Niño3.4 response removed (Figure 2) shows surface-intensified warming exceeding  $0.12^{\circ}\text{C decade}^{-1}$  at its surface maximum and remains positive over the entire pressure range of 0–1975 dbar. The spatial pattern of OCHA trend over 0–1975 dbar (Figure 4) is similar to that previously reported for 2006–2013 [Roemmich et al., 2015], although there are differences, especially in the tropical Pacific and the subpolar North Atlantic. The latter region shows a stronger cooling in the present analysis, owing to the recent very cold conditions there [Duchez et al., 2016], which were not included in the previous study. Here the western tropical Pacific decadal trend is toward cooling and the eastern tropical Pacific warms, whereas the opposite pattern holds for the 2006–2013 analysis [Roemmich et al., 2015]. The previous analysis

also removes ENSO, although with a different technique, so again the different time periods may cause the differences. Elsewhere, the patterns look similar: the Indian Ocean warms in the north but cools at latitudes near Madagascar. As reported previously [Wu *et al.*, 2012], all the subtropical western boundary current extension waters near the Gulf Stream, Kuroshio, Brazil, East Australia, and Agulhas currents warm more than their surroundings. There is a strong Southern Hemisphere warming centered at about 40°S. Roughly 9/10 of net global warming trend presented here is found in the Southern Hemisphere, similarly to results from three different analyses for January 2006 to November 2015 [Wjiffels *et al.*, 2016].

## 5. Discussion

Decade-long records of OHCA and TOA net energy storage allow the removal of a reliable seasonal cycle, and exploration of the global heat budget in relation to ENSO. Previous studies based on shorter records or earlier observation systems have come to various conclusions on the phase relation between TOA net energy flux and ENSO [Loeb *et al.*, 2012; Roemmich and Gilson, 2011; Wong *et al.*, 2006]. Here we demonstrate a strong zero-time lag correlation between TOA net energy storage and Niño3.4, with Earth's energy storage anomalies (mostly within the ocean) peaking in phase with El Niño. This result is consistent with a recent analysis of global sea level variations [Piecuch and Quinn, 2016]. While this net energy storage modulation can be large on interannual time scales, for the 2005–2015 period the trend in Niño3.4 is about  $0.054^{\circ}\text{C yr}^{-1}$ , implying only a  $0.01 \text{ W m}^{-2}$  bias owing to ENSO variability for a recent  $0.71 \text{ W m}^{-2}$  TOA net energy flux estimate [Johnson *et al.*, 2016]. Thus, ENSO appears to have a much smaller impact on long-term global energy storage trends than it does on long-term global surface temperature trends [Foster and Rahmstorf, 2011]. However, some potentially spurious local correlations such as the implied ocean cooling of the subpolar North Atlantic during El Niño remain. Longer records will reduce uncertainties further.

While it is not possible to investigate decadal modes of variability from time series that are not much longer than a decade, these modes, such as the PDO [England *et al.*, 2014] and the North Atlantic Oscillation [Marshall *et al.*, 2001], are also important in modulating climate. For example, the phase of the PDO, which may have been influenced by anthropogenic aerosols in the 2000s [Smith *et al.*, 2016], appears to modulate the decadal rate of global surface temperature rise [Kosaka and Xie, 2013], sea level rise [Hamlington *et al.*, 2013], and even global energy uptake, with the latter a prediction from climate models [Xie *et al.*, 2016]. These studies suggest a decreased rate of global ocean warming (as well as surface temperature and sea level increases) during the transitions from the warm to the cool phase of the PDO, as occurred around 1998. The 2014 transition to a warm phase of the PDO may reverse that effect. Extending CERES and Argo records over decadal time scales, augmented by Deep Argo as it develops [Johnson *et al.*, 2015], will allow the decadal modulations of Earth's energy imbalance, predicted by climate models, to be estimated directly from observations.

## Acknowledgments

Argo data were collected and made freely available by the International Argo Program and the national programs that contribute to it (<http://www.argo.ucsd.edu> and <http://argo.jcom-mops.org>). The Argo Program is part of the Global Ocean Observing System. Data used in this study can be accessed at the URLs found in section 2. We thank two anonymous reviewers for their helpful comments. G.C.J. is supported by the Climate Observation Division, Climate Program Office, National Oceanic and Atmospheric Administration (NOAA), U.S. Department of Commerce, and NOAA Research. A.N.B. was supported by the NOAA Hollings Scholar Program. Pacific Marine Environmental Laboratory Contribution Number 4557.

## References

- Blunden, J., and D. S. Arndt (2016), State of the climate in 2015, *Bull. Am. Meteorol. Soc.*, 97(8), doi:10.1175/2016BAMSStateoftheClimate.1.
- Cazenave, A., O. Henry, S. Munier, T. Delcroix, A. L. Gordon, B. Meyssignac, W. Llovel, H. Palanisamy, and M. Becker (2012), Estimating ENSO influence on the global mean sea level, 1993–2010, *Mar. Geodyn.*, 35, 82–97, doi:10.1080/01490419.2012.718209.
- Ciasto, L. M., G. R. Simpkins, and M. H. England (2015), Teleconnections between tropical Pacific SST anomalies and extratropical Southern Hemisphere climate, *J. Clim.*, 28(1), 56–65, doi:10.1175/jcli-d-14-00438.1.
- Duchez, A., E. Frajka-Williams, S. A. Josey, D. G. Evans, J. P. Grist, R. Marsh, G. D. McCarthy, B. Sinha, D. I. Berry, and J. J. M. Hirschi (2016), Drivers of exceptionally cold North Atlantic Ocean temperatures and their link to the 2015 European heat wave, *Environ. Res. Lett.*, 11(7), 9, 074004, doi:10.1088/1748-9326/11/7/074004.
- England, M. H., S. McGregor, P. Spence, G. A. Meehl, A. Timmermann, W. Cai, A. Sen Gupta, M. J. McPhaden, A. Purich, and A. Santoso (2014), Recent intensification of wind-driven circulation in the Pacific and the ongoing warming hiatus, *Nat. Clim. Change*, 4(3), 222–227, doi:10.1038/nclimate2106.
- Fasullo, J. T., C. Boening, F. W. Landerer, and R. S. Nerem (2013), Australia's unique influence on global sea level in 2010–2011, *Geophys. Res. Lett.*, 40, 4368–4373, doi:10.1002/grl.50834.
- Foster, G., and S. Rahmstorf (2011), Global temperature evolution 1979–2010, *Environ. Res. Lett.*, 6(4), 8, doi:10.1088/1748-9326/6/4/044022.
- Hamlington, B. D., R. R. Leben, M. W. Strassburg, R. S. Nerem, and K. Y. Kim (2013), Contribution of the Pacific Decadal Oscillation to global mean sea level trends, *Geophys. Res. Lett.*, 40, 5171–5175, doi:10.1002/grl.50950.
- Intergovernmental Oceanographic Commission, SCOR, and IAPSO (2010), The international thermodynamic equation of seawater – 2010: Calculation and use of thermodynamic properties, Intergovernmental Oceanographic Commission, Manuals and Guides No. 56, 196 pp., UNESCO.
- Johnson, G. C., J. M. Lyman, and S. G. Purkey (2015), Informing Deep Argo array design using Argo and full-depth hydrographic section data, *J. Atmos. Oceanic Technol.*, 32(11), 2187–2198.
- Johnson, G. C., J. M. Lyman, and N. G. Loeb (2016), Improving estimates of Earth's energy imbalance, *Nat. Clim. Change*, 6(7), 639–640.
- Kosaka, Y., and S. P. Xie (2013), Recent global-warming hiatus tied to equatorial Pacific surface cooling, *Nature*, 501(7467), 403–407, doi:10.1038/nature12534.

- Loeb, N. G., J. M. Lyman, G. C. Johnson, R. P. Allan, D. R. Doelling, T. Wong, B. J. Soden, and G. L. Stephens (2012), Observed changes in top-of-the-atmosphere radiation and upper-ocean heating consistent within uncertainty, *Nat. Geosci.*, *5*(2), 110–113, doi:10.1038/ngeo1375.
- Lumpkin, R., and G. C. Johnson (2013), Global ocean surface velocities from drifters: Mean, variance, El Niño–Southern Oscillation response, and seasonal cycle, *J. Geophys. Res. Oceans*, *118*, 2992–3006, doi:10.1002/jgrc.20210.
- Lyman, J. M., and G. C. Johnson (2014), Estimating global ocean heat content changes in the upper 1800 m since 1950 and the influence of climatology choice, *J. Clim.*, *27*(5), 1945–1957, doi:10.1175/jcli-d-12-00752.1.
- Marshall, J., Y. Kushner, D. Battisti, P. Chang, A. Czaja, R. Dickson, J. Hurrell, M. McCartney, R. Saravanan, and M. Visbeck (2001), North Atlantic climate variability: Phenomena, impacts and mechanisms, *Int. J. Climatol.*, *21*(15), 1863–1898, doi:10.1002/joc.693.
- McPhaden, M. J., S. E. Zebiak, and M. H. Glantz (2006), ENSO as an integrating concept in Earth science, *Science*, *314*(5806), 1740–1745, doi:10.1126/science.1132588.
- Meinen, C. S., and M. J. McPhaden (2000), Observations of warm water volume changes in the equatorial Pacific and their relationship to El Niño and La Niña, *J. Clim.*, *13*(20), 3551–3559, doi:10.1175/1520-0442(2000)013<3551:ooowwvc>2.0.co;2.
- Newman, M., et al. (2016), The Pacific Decadal Oscillation, revisited, *J. Clim.*, *29*(12), 4399–4427, doi:10.1175/jcli-d-15-0508.1.
- Pieuch, C. G., and K. J. Quinn (2016), El Niño, La Niña, and the global sea level budget, *Ocean Sci.*, *12*(6), 1165–1177, doi:10.5194/os-12-1165-2016.
- Rhein, M., et al. (2013), Observations: Ocean, in *Climate Change 2013: The Physical Science Basis. Contribution of Working Group I to the Fifth Assessment Report of the Intergovernmental Panel on Climate Change*, edited by T. F. Stocker et al., pp. 255–315, Cambridge Univ. Press, Cambridge, U. K., and New York, doi:10.1017/CBO9781107415324.010.
- Roemmich, D., and J. Gilson (2009), The 2004–2008 mean and annual cycle of temperature, salinity, and steric height in the global ocean from the Argo Program, *Prog. Oceanogr.*, *82*(2), 81–100, doi:10.1016/j.pocean.2009.03.004.
- Roemmich, D., and J. Gilson (2011), The global ocean imprint of ENSO, *Geophys. Res. Lett.*, *38*, L13606, doi:10.1029/2011GL047992.
- Roemmich, D., J. Church, J. Gilson, D. Monselesan, P. Sutton, and S. Wijffels (2015), Unabated planetary warming and its ocean structure since 2006, *Nat. Clim. Change*, *5*(3), 240–245, doi:10.1038/nclimate2513.
- Smith, D. M., B. B. Booth, N. J. Dunstone, R. Eade, L. Hermanson, G. S. Jones, A. A. Scaife, K. L. Sheen, and V. Thompson (2016), Role of volcanic and anthropogenic aerosols in the recent global surface warming slowdown, *Nat. Clim. Change*, *6*(10), 936–940, doi:10.1038/nclimate3058.
- Sprintall, J., A. L. Gordon, A. Koch-Larrouy, T. Lee, J. T. Potemra, K. Pujiana, and S. E. Wijffels (2014), The Indonesian seas and their role in the coupled ocean–climate system, *Nat. Geosci.*, *7*(7), 487–492, doi:10.1038/ngeo2188.
- Trenberth, K. E., and D. P. Stepaniak (2001), Indices of El Niño evolution, *J. Clim.*, *14*(8), 1697–1701, doi:10.1175/1520-0442(2001)014<1697:lioeno>2.0.co;2.
- Trenberth, K. E., J. M. Caron, and D. P. Stepaniak (2001), The atmospheric energy budget and implications for surface fluxes and ocean heat transports, *Clim. Dyn.*, *17*(4), 259–276, doi:10.1007/pl00007927.
- Trenberth, K. E., J. T. Fasullo, K. von Shuckmann, and L. Cheng (2016), Insights into Earth’s energy imbalance from multiple sources, *J. Clim.*, doi:10.1175/JCLI-D-16-0339.1.
- Wang, H., and V. M. Mehta (2008), Decadal variability of the Indo-Pacific warm pool and its association with atmospheric and oceanic variability in the NCEP–NCAR and SODA Reanalyses, *J. Clim.*, *21*(21), 5545–5565, doi:10.1175/2008jcli2049.1.
- Wijffels, S., D. Roemmich, D. Monselesan, J. Church, and J. Gilson (2016), Ocean temperatures chronicle the ongoing warming of Earth, *Nat. Clim. Change*, *6*(2), 116–118.
- Wong, T., B. A. Wielicki, R. B. Lee, G. L. Smith, K. A. Bush, and J. K. Willis (2006), Reexamination of the observed decadal variability of the earth radiation budget using altitude-corrected ERBE/ERBS nonscanner WFOV data, *J. Clim.*, *19*(16), 4028–4040, doi:10.1175/jcli3838.1.
- Wu, L. X., et al. (2012), Enhanced warming over the global subtropical western boundary currents, *Nat. Clim. Change*, *2*(3), 161–166, doi:10.1038/nclimate1353.
- Xie, S. P., Y. Kosaka, and Y. M. Okumura (2016), Distinct energy budgets for anthropogenic and natural changes during global warming hiatus, *Nat. Geosci.*, *9*(1), 29–33, doi:10.1038/ngeo2581.